Available online at www.sciencedirect.com

ScienceDirect

journal homepage: www.elsevier.com/locate/he

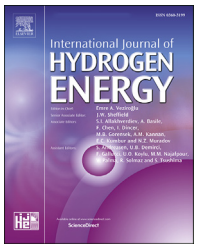

Initial approaches in benchmarking and round robin testing for proton exchange membrane water electrolyzers

G. Bender [a] *, M. Carmo [b], T. Smolinka [c], A. Gago [d], N. Danilovic [e,1], M. Mueller [b], F. Ganci [a,f], A. Fallisch [c], P. Lettenmeier [d], K.A. Friedrich [d], K. Ayers [e], B. Pivovar [a], J. Mergel [g], D. Stolten [b,h]

[a] National Renewable Energy Laboratory, Golden CO 80401, USA
[b] Forschungszentrum Jülich GmbH, IEK-3: Electrochemical Process Engineering, 52425 Jülich, Germany
[c] Fraunhofer Institute for Solar Energy Systems ISE, D-79110 Freiburg, Germany
[d] Institute of Engineering Thermodynamics, German Aerospace Center, Pfaffenwaldring 38-40, Stuttgart, 70569, Germany
[e] Proton OnSite, 10 Technology Drive, Wallingford, CT 06492, USA
[f] University of Palermo, 90128 Palermo, Italy
[g] Jülich, Operating Agent IEA Electrolysis Annex 30, Germany
[h] Chair for Fuel Cells, RWTH Aachen University, Germany

ARTICLE INFO

Article history:
Received 31 August 2018
Received in revised form
6 February 2019
Accepted 10 February 2019
Available online 15 March 2019

Keywords:
Electrolysis
PEMWE
Benchmarking
Round robin
State-of-the-art
Protocol development

ABSTRACT

As ever-increasing amounts of renewable electricity enter the energy supply mix on a regional, national and international basis, greater emphasis is being placed on energy conversion and storage technologies to deal with the oscillations, excess and lack of electricity. Hydrogen generation via proton exchange membrane water electrolysis (PEMWE) is one technology that offers a pathway to store large amounts of electricity in the form of hydrogen. The challenges to widespread adoption of PEM water electrolyzers lie in their high capital and operating costs which both need to be reduced through R&D. An evaluation of reported PEMWE performance data in the literature reveals that there are excessive variations of in situ performance results that make it difficult to draw conclusions on the pathway forward to performance optimization and future R&D directions. To enable the meaningful comparison of in situ performance evaluation across laboratories there is an obvious need for standardization of materials and testing protocols. Herein, we address this need by reporting the results of a round robin test effort conducted at the laboratories of five contributors to the IEA Electrolysis Annex 30. For this effort a method and equipment framework were first developed and then verified with respect to its feasibility for measuring water electrolysis performance accurately across the various laboratories. The effort utilized identical sets of test articles, materials, and test cells, and employed a set of shared test protocols. It further defined a minimum skeleton of requirements for the test station equipment. The maximum observed deviation between laboratories at 1 A cm^{-2} at cell temperatures of 60 °C and 80 °C was 27 and 20 mV, respectively. The deviation of the results from laboratory to laboratory was 2–3 times higher than the lowest deviation observed at one single lab and test station. However, the

* *Corresponding author.*
E-mail address: guido.bender@nrel.gov (G. Bender).
[1] Present address: Lawrence Berkeley National Laboratory, Berkeley, CA 94720, USA.
https://doi.org/10.1016/j.ijhydene.2019.02.074

highest deviations observed were one-tenth of those extracted by a literature survey on similar material sets. The work endorses the urgent need to identify one or more reference sets of materials in addition to the method and equipment framework introduced here, to enable accurate comparison of results across the entire community. The results further imply that cell temperature control appears to be the most significant source of deviation between results, and that care must be taken with respect to break-in conditions and cell electrical connections for meaningful performance data.

Introduction

Polymer electrolyte membrane water electrolysis (PEMWE) is a commercially available technology used to produce hydrogen and oxygen. It was developed in the 1960–1970s by General Electric as an alternative to conventional alkaline electrolyzers [1,2]. The development of proton conductive perfluorosulfonic acid (PFSA) polymers by DuPont led to the use of a solid membrane working as both an electrolyte and gas separator inside the cell. The integration of the polymer electrolyte membrane (PEM) enabled the reduction of ohmic losses and gas permeation, enabled operation at high differential pressures and removed caustic liquid electrolyte. Many challenges surfaced when operating in an acidic environment at potentials above 1.23 V, which is the standard onset potential for the oxygen evolution reaction. These conditions demand the use of corrosion-resistant materials beyond what was used at the time in alkaline electrolyzers. Thus, nickel catalysts and stainless-steel porous transport layers (PTLs) and bipolar plates (BPs) were replaced by platinum group metal (PGMs) catalysts and titanium PTLs and BPs in today's commercial systems. While PEM water electrolyzers are commercially available they were developed for niche applications such as life support applications and industrial gas supply where reliability is the key driver, not cost. Consequently, even to this date, systems are overdesigned with high catalyst loadings, PGM-coated titanium components and thick PFSA membranes. To achieve significant market penetration of PEM electrolyzers in the energy sector, the investments costs (CAPEX) and operational costs (OPEX) will have to result in hydrogen cost of 2$/kg or less according to the United States Department of Energy 2020 hydrogen production cost target [3,4]. Furthermore, the technology will have to reach lifespans over 40,000 h and provide adequate reliability in order to obtain market acceptance. These targets can only be reached through strong investments in R&D efforts.

Since the initial PEMWE development, significant improvements in cell performance, efficiency and durability have been reported [5–9]. Today's R&D efforts by industry, academia and research institutions are manifold. They target further capital cost reduction through lowering of the catalyst loading [10], improving BP and PTL manufacture and coating processes [11–15], and developing alternative membrane materials [16]. Unfortunately, the reported results for PEMWE cells that are present in the literature are very difficult to compare. Fig. 1 shows the cell voltages for three different membrane materials at various current densities extracted from approximately 200 publications. Across the literature, the performance at 1 A cm^{-2} deviates up to 600 mV. Lower deviations were observed with thicker membrane materials, for example, the variation at 1 A cm^{-2} for Nafion 117 was 200 mV. In any case, the magnitude of deviation is unacceptable for determining state-of-the-art and comparing results across institutions.

Other areas have faced similar challenges in the past, the field of proton exchange membrane fuel cells (PEMFCs) being probably the most related to PEMWE. In the early 2000's first attempts in the United States (US) on harmonizing in-situ testing were published by the Single Cell Testing Task Force of the US Fuel Cell Council (USFCC). Standards for test station equipment were established in the "Fuel Cell Test Station Requirements and Verification Procedure" [17] and testing protocols were described in the document "Single Cell Test Protocol" [18]. The latter was not necessarily recommending standard hardware for testing materials but suggested that "the procedures and hardware may be useful in cases where adopting an existing, non-proprietary protocol would expedite inter-lab data qualification as a basis for other data exchange" [18]. The approach may have led to the adoption and implementation of standard operating procedures into the Multi-Year Research, Development, and Demonstration (MYRDD) Plan [19] from the US Department of Energy (DOE) Fuel Cell Technology Office (FCTO). This document describes the goals, objectives, technical targets, tasks, and schedules for all activities within the FCTO. It is a living document that further specifies testing protocols for fuel cells and fuel cell components, that were developed in partnership with the U.S. DRIVE Fuel Cell Technical Team. These protocols became essential for demonstrating material performance for DOE funded fuel cell projects.

Because PEMWE is not as maturely developed as PEMFC, the challenges that the community faces to compare data are similar to those fuel cells faced in the early 2000s. The deviation in performance discussed above is directly related to the large variety of materials, cell or stack components, surface treatments, catalyst loadings, and the applied method and equipment framework, i.e. test station configurations, operating conditions and operating procedures used. A common (i.e. harmonized) approach for performance testing that enables more direct comparison of results between institutions would be highly beneficial for the development of novel materials and components. Such an approach would require (i) a measurement method consisting of operating conditions and

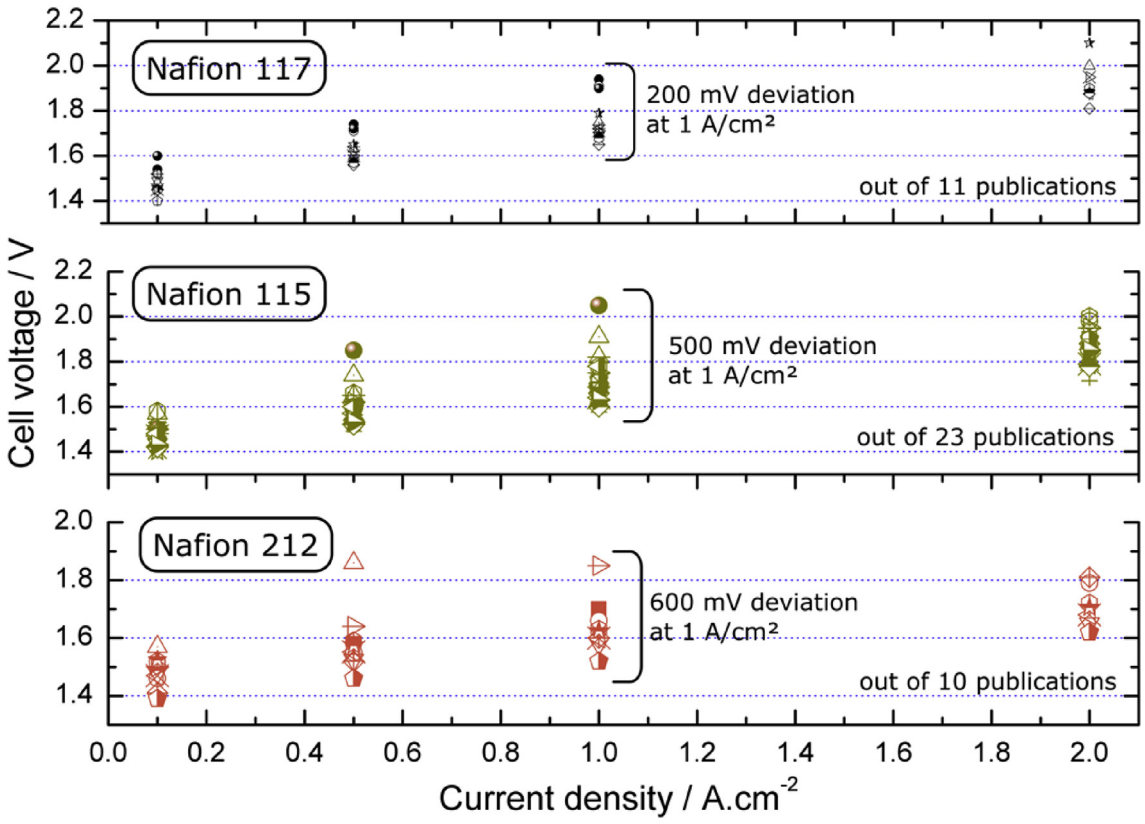

Fig. 1 – Distribution of performance results extracted from the literature [5,15,20–88] for cells with N117, N115, or NR-212 Nafion membranes.

procedures, (ii) an equipment framework that describes minimum test station requirements, and (iii) the selection of one or more reference material sets (membrane, catalyst, loading, GDLs, and hardware). This work focuses on items (i) and (ii) using a temporary solution for item (iii), which will be the focus of future work.

If one considers the great majority of publications on PEMWE, commonly used materials and components can be identified, such as iridium oxide as anode catalyst and Nafion membranes as electrolyte. This enables a classification of current state-of-the art materials for PEMWE. Table 1 shows a list of commonly used materials and components together with parameters that may impact the cell's performance and durability. Though the material choices were similar, strong variation in intrinsic properties such as surface area, porosity, mass transport, electron and proton conductivity, corrosion resistance, and activity may have contributed to the variations observed in the literature data that are displayed in Fig. 1. Moreover, the beneficial effects of functional coatings and engineering aspects such as hardware design and size, flow-field geometry, clamping forces and thus contact resistances and thermal management may also play a key role in determining the cell performance. And last not least, the use of different cell operating conditions including temperature, pressure, water flow rates, and water quality make the desired meaningful performance comparison of materials from literature data essentially impossible.

The development of widely accepted benchmarks, reference operating conditions and operation procedures are key to promote meaningful comparison across internal research efforts which will accelerate the development and market penetration of advanced PEMWE technology. This work is an initial effort to start the process toward such a comparison platform.

The overall goal of this work is to establish a method that enables straightforward evaluation of baseline or state-of-the-art materials for PEMWE and to validate it with accurate performance comparison. In the process trust is established between different institutions, domestic and international collaborations are promoted, and most importantly it leads to selective research efforts that will accelerate the development of PEMWE technologies and foster the adoption of novel concepts by the industry. We present here the methodology and data from a round robin testing effort that is intended to serve as a sound foundation for such a data comparison.

Methodology

The chosen methodology was based on the commitment, motivation and collective experience of the participating institutions: National Renewable Energy Laboratory (NREL), Forschungszentrum Jülich (FZ-Jülich), Fraunhofer Institute for Solar Energy Systems (ISE), German Aerospace Center (DLR) and Proton Onsite. A short turnaround time of less than a year

Table 1 – List of PEMWE components/materials and the potential variations in the design parameters.

Component	Material	Potential Variations
Membrane	Nafion	Thickness Equivalent weight Conductivity Gas permeation Processing conditions
Anode & Cathode Catalyst/Electrode	IrOx Pt/C	Activity Stability Surface area Ionomer content Porosity Thermal & electrical conductivity Catalyst loading Water transport
Anode & Cathode PTL	(Coated) Titanium Carbon Paper	Protective coating Hydrophobic coating Porosity Thickness Thermal & electrical conductivity Passivation Pore sizes Roughness
Anode & Cathode Flow Field Material	(Coated) Titanium Graphite (Composite)	Protective coating Functional coating Thermal & electrical conductivity Geometry Passivation

was targeted so that results could be offered to the community for adoption in a very reasonable time frame. For time-saving purposes, a parallel, rather than a sequential, experimental approach was chosen. The work presented here was divided into two phases:

- Phase 1: Prior to testing, all participating institutions received identical PEMWE cell hardware, with five sets of PTLs, gaskets and CCMs (all courtesy of FZ Jülich). Experimental test conditions, such as assembly torque, water flow, outlet pressure, temperature, and test protocols were decided upon and carefully communicated to the institutions. The measurements were performed at each institution within approximately the same time frame using either commercial or built-in-house test stations. Minimal test station requirements were defined for the round robin experiments. All test stations were expected to be fully calibrated with each laboratory following their own routines and procedures. Measurements included cell conditioning, current controlled performance curves, and electrochemical impedance spectroscopy (EIS) measurements. The data were subsequently collected and processed, analyzed and prepared for reporting at FZ Jülich and NREL.
- Phase 2: Based on some of the results, specific measurements were repeated after some corrective actions, such as temperature calibration, were applied. An effort was made to understand variability within a single lab and in between multiple labs by looking at statistical variation (standard deviation) and the occurrence of outlying measurements. Specific diagnostics like temperature measurements and high frequency resistance were also used to probe the source of measurement uncertainties. The results were analyzed, and conclusions were reached.

Experimental

For this work, all materials and components were intentionally used "as received". The different laboratories did not receive any instructions on how to handle and/or treat the materials and components used for the round robin test. A set of essential but simple instruction was communicated that can be performed with any standard laboratory setting for PEM water electrolysis testing. Typical laboratory procedures such as calibration, sample handling with gloves and providing a typical safety frame work were expected. Out of the ordinary laboratory capabilities such as sputter coating of material were not considered to be performed at each laboratory. This work is a first step at understanding which minimal set of requirements provides maximal measurement agreement.

Hardware

The meaningful comparison of data across laboratories requires harmonization of test procedures as well as the utilization of the same cell hardware. Standardized commercially available off-the-shelf hardware would be ideal for comparison purposes. At the time of this study neither an agreement on harmonized test procedures nor a commonly used commercial PEM water electrolyzer cell was available on the market. To allow for progress in the harmonization process without access to a widely accepted reference hardware, FZ

Jülich provided complete sets of an available "arbitrary" 25 cm^2 cell hardware to each participating laboratory. Choosing this hardware enabled that each lab could conduct testing without delay using identical cell design and material. Future work will address evaluation of single cell R&D hardware configurations to identify a material and hardware combination that can serve as a reference system to the community.

As shown in Fig. 2(a) and (b), the hardware featured a typical R&D single cell design: thick endplates for compression with 6 bolts, gold-plated copper current collector plates, and pin-cushion flow-fields with distributed flow inlet and outlets. The anode and cathode flow fields were platinum and platinum/gold-plated titanium, respectively. The overall flow-field size was 95 mm × 95 mm, the active area was 50 mm × 50 mm, and the flow-field consisted of evenly spaced 1.7 mm × 1.7 mm pins. The hardware featured 4 mm voltage sense ports, cartridge heater ports and flow inlets and outlets integrated into the flow-fields. Instead of the voltage sense ports, alligator-clip-type connections could be used on the current collector plate.

The temperature of the cell during operation was typically controlled by the flow of heated water supplied to the cell. Water and water/gas temperatures were sensed at the cell inlet and outlet. The type of temperature control, feedback, sensor type and exact sensing location depended on each laboratory's setup and available equipment. The temperature setpoint was defined as the cell inlet temperature. In addition, optional cartridge heaters that were inserted into the flow-field plates or optional pad heaters that were glued onto the endplates were used by certain participants to heat the cell. In this case a thermocouple was inserted into the hardware and used as the temperature control point for the cell. Cell assembly was performed with a torque of 8 Nm using a minimum of two steps (4 and 8 Nm) to ramp up the torque. This created a compression force of about 2 MPa at the pin cushion flow-field.

Catalyst-coated membrane, gaskets and PTLs

The catalyst-coated membranes (CCMs) used in this work were the commercially available product E300 from Greenerity GmbH. These CCMs were fabricated using Nafion N117 membranes, iridium-based anodes with a nominal loading of 2.5 mg_{Ir} cm^{-2} and platinum-based cathodes with a nominal loading of 0.8 mg_{Pt} cm^{-2}. The electrode area of 53 mm × 53 mm was centered on the membrane area of 95 mm × 95 mm. The active area of the CCMs was defined as 25 cm^2 based on the PTL and flow-field geometry. CCMs, gasket and PTL materials were provided by FZ Jülich. Gaskets

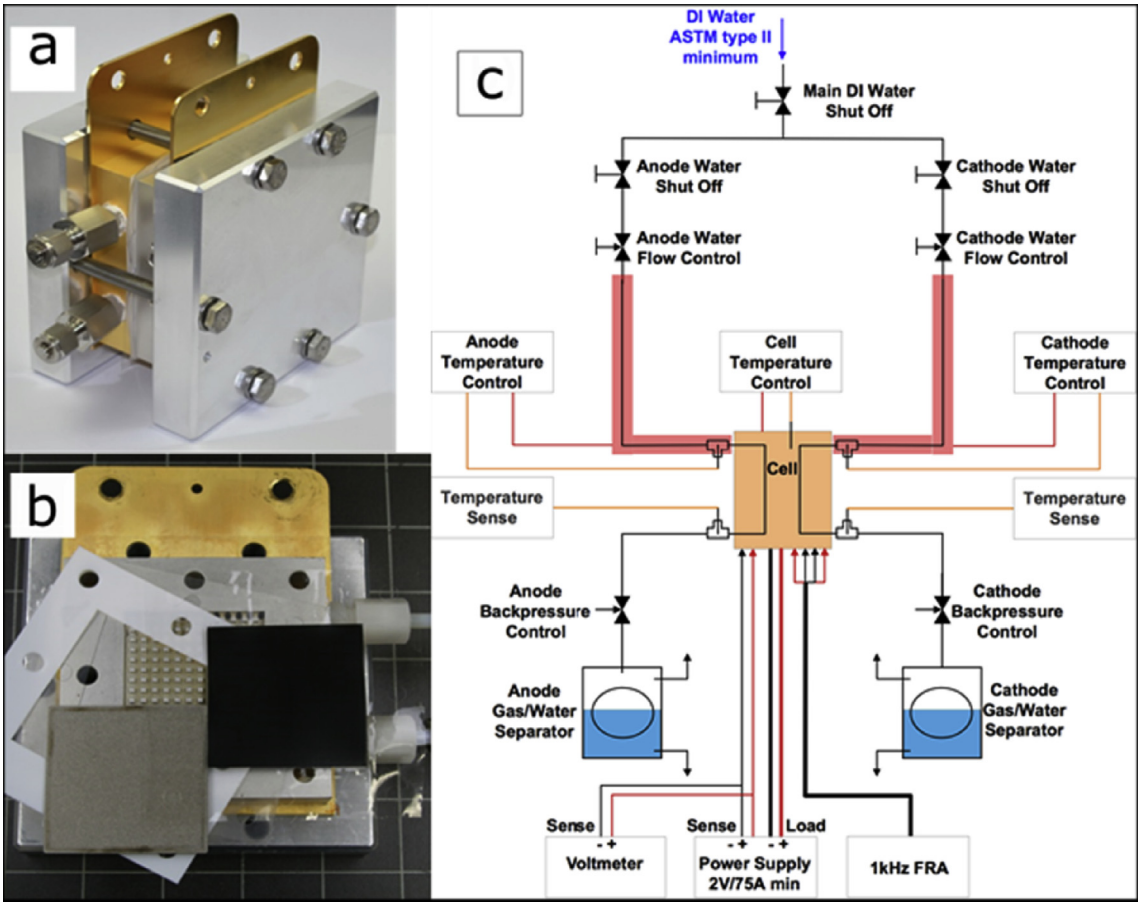

Fig. 2 – a) Round robin hardware cell and b) components featuring pin-cushion flow-field, carbon fiber-based PTL and N117 CCM with Ir and Pt based catalyst layers. c) Schematic of bare bones test station equipment necessary to meet minimum requirements for test procedure.

consisted of 250 μm thick skived PTFE. The gasketing window was 51 mm × 51 mm. For both PTLs carbon paper TGP-H-120 from Toray, with a thickness of 370 μm and 5% PTFE loading, was applied, despite its low corrosion resistance at high potentials at the anode side. Typically, titanium-based PTLs are used on the anode side of PEMWE cells. For the short-term performance experiments performed in this study, we decided to use the well-defined, cost-effective, and readily available carbon paper instead of Ti-PTL materials. Carbon paper is acceptably stable as a PTL for the anode of the PEM electrolyzer cell when the duration of the experiments is less than 20 h (work in progress).

Station requirements and operating conditions

Test stations were expected to be fully calibrated. Each laboratory was left to use their own standard routines and procedures for calibration. A schematic of the minimum test station equipment required for carrying out the measurements is presented in Fig. 2(c). It consists of a deionized water supply for water single pass operation, shut-off and flow-control valves for the water, temperature control of the water and the cell, water/gas separation and exhaust, electrical power supply, and voltage sense. The backpressure control system shown in the figure is required only for laboratories located at high elevation (i.e., wherever ambient pressures are below 1 bar, the ambient pressure at sea level).

The operating conditions that were applied during the round robin experiments are summarized in Table 2. Deionized water with a quality standard of ASTM Type II (i.e., a minimum resistance of 1 MΩ cm) was flowed through the cell at the anode side and could optionally also be flowed through the cathode side. Flow direction was from the bottom to the top of the flow-field to promote bubble removal during operation. The flow rate was, at a minimum, 2 mL min^{-1} cm^{-2} geometric electrode area (i.e. 50 ml min^{-1} for the 25 cm^2 cell).

When flowing, the water temperature was controlled to the cell inlet, ideally using a temperature sensor placed in the center of the water flow at the anode as shown in Fig. 2(c). The outlet water temperature was measured in the same way. As mentioned before, the type of temperature control, feedback, sensor type and exact sensing location depended on each laboratory's setup and available equipment. However, when the cell was heated and operated, the differential temperature between cell inlet and cell outlet was required to be less than 2 K. Experiments were performed at two operating temperatures: 60 °C and 80 °C. Anode and cathode outlet pressures each were 1 bar absolute. Operation at 1 bar absolute required no active pressure control at most contributing laboratories. At high elevations such as Golden, Colorado, USA, where NREL is located, the ambient pressure is approximately 0.83 bar and an active pressure control was employed to reach the desired operating pressure. For this work NREL used electro-pneumatic transducers TT7800-705 from Fairchild combined with M20 forward/exhaust flow volume boosters from Fairchild. The system allows accurate adjustment of pressure up to 4 bar absolute and works with liquid as well as gaseous flows.

The test stations further required a minimum 150 W power supply with current capability of 75 A (i.e. 3 A cm^{-2} at 2 V). Though not specified, it was expected that each laboratory would follow best practice and use a four-wire measurement setup with separate voltage sense lines. High-frequency resistance (HFR) measurements were also desired. The setup and instrumentation used for HFR measurements can vary significantly. Setup configurations may consist of fixed frequency 1 kHz measurement instruments that measure the impedance while the power supply is controlling the cell current, or they may use frequency response analyzers (FRA) with variable frequencies and a potentiostat/galvanostat combined with a current booster. The setup and instrument specifics determine the current range at which the experiment can be conducted. Minimum measurement specifications included conducting a 1 kHz impedance measurement at a current density of 50 mA cm^{-2}. The choices for equipment and measurement strategy for conducting HFR and/or EIS measurements were left up to each laboratory. Extending the EIS experimental scope from the 1 kHz HFR measurement to other frequencies and current densities was of interest, but optional. If a laboratory was conducting EIS experiments, it was free to pick any frequency range they were interested in as long as it contained 1 kHz. For the HFR/EIS measurement the perturbation was supposed to be ±5% of the applied current, without exceeding ±10 mV of the applied voltage. For the determination of the 1 kHz HFR the phase shift was expected to be below ±5°.

Table 2 – Standard operating conditions applied during round robin test effort.

Condition	Set Point
Cell Temperature	60, 80 °C
Water Flow Temp. Anode	60, 80 °C (inlet)
Water Flow Temp. Cathode	60, 80 °C (inlet) Flow is optional
Minimum Water Flow Anode	2 mL cm^{-2} min^{-1} $\Delta T \leq 2$ K
Minimum Optional Water Flow Cathode	2 mL cm^{-2} min^{-1} $\Delta T \leq 2$ K
Outlet Pressure Anode	1 bar absolute
Outlet Pressure Cathode	1 bar absolute
Water Quality	ASTM Type II (>1 MΩ cm)
Power Supply Maximum Current	≥ 75 A
Power Supply Maximum Voltage	≥ 2 V
EIS	Minimum 1 kHz

Conditioning and operating procedures

The operating procedures used for conducting the round robin tests are summarized in Table 3. Experiments were typically conducted at 60 °C first, then at 80 °C. Each CCM required conditioning at each temperature. The cells were warmed up by applying temperature set points to the water flowing through the cell (i.e., the water flowing through the anode, and—if available—through the cathode). Once the temperatures were established, a current density of 0.2 A cm^{-2} was applied to the cell for 30 min. Subsequently, the current density was increased to 1.0 A cm^{-2} for another 30 min. Then the cell was operated at a constant cell voltage of 1.7 V until the cell current variation became smaller than 1% per hour. At a

Table 3 – Operating procedure for round robin test effort at 60 and 80 °C.

Step	Description	Specifications
Warm Up	Apply flows and temperatures until operating conditions stabilized	1) Water and cell temperatures: 60 °C or 80 °C 2) Water flow of 2 mL cm^{-2} min^{-1} into cathode and optionally into anode with $\Delta T \leq 2$ K
Cell Conditioning	Condition cell using manufacturer break-in procedure	1) 30 min at 0.2 A cm^{-2} current controlled operation 2) 30 min at 1 A cm^{-2} current controlled operation 3) 1.7 V voltage controlled operation until variation is less than 1% per hour
Performance Evaluation	Conduct current controlled VI curves up to a cell voltage of 2 V	1) Low to high current density curve • Step duration = 5 min • Step size of Δi = 0.02 mA cm^{-2} from 0.0 to 0.1 mA cm^{-2} • Step size of Δi = 0.2 mA cm^{-2} from 0.2 mA cm^{-2} on until a voltage of 2.0 V is reached 2) High to low current density curve • Reverse current steps from 1) 3) Optional OCV measurement after VI curves
HFR Evaluation	Conduct 1 kHz HFR measurements	• ± 5% of DC load current • ΔV not to exceed ±10 mV • $\lvert\varphi\rvert \leq 5°$ • Minimum 1 kHz at 0.05 mA cm^{-2} • Optional EIS spectra at all current densities at frequency range up to 0.1 Hz–10 kHz

cell temperature of 60 °C the conditioning of an unused CCM is expected to take up to 12 h. Subsequently, performance curves were conducted using 5-min steps. Starting from open circuit the current was increased in 20 mA cm^{-2} steps up to 100 mA cm^{-2}. The next current density was 200 mA cm^{-2} and current densities were stepped up in 200 mA cm^{-2} steps until a maximum cell voltage of 2.0 V was reached. Current densities were stepped down again, using the same current density steps. Optionally, the open circuit voltage (OCV) was recorded after the last step.

In addition to the performance data, HFR data were collected either during the performance curves or in separate experiments. The HFR for this comparison effort is defined as the real part of the 1 kHz impedance. The measurement should at most use a current perturbation of ±5% of the cell current and a maximum voltage perturbation of 10 mV. The resulting HFR was acceptable when the phase shift of the complex impedance was below ±5°. Impedance spectra were additionally collected when available at the laboratory at select current densities. The spectra typically ranged between 0.1 Hz and 10 kHz and used the same experimental conditions as described for the HFR experiments.

Results & discussion

In this section the results obtained with the cell hardware distributed to the five different laboratories are presented. It is irrelevant for the interpretation of the results of the round robin test to specify which laboratory provided a given data set. Therefore, the legends in the figures will only state Lab1, Lab2, Lab3, Lab4 and Lab5.

Fig. 3(a) shows the anode endplate temperatures of three CCMs measured by one laboratory during the cell warm up and Fig. 3(b) shows performance data during the last step of cell conditioning. The temperature profile during the warm up was reproducible for all three CCMs. The cell temperature rapidly increased toward the 80 °C target temperature. All cell

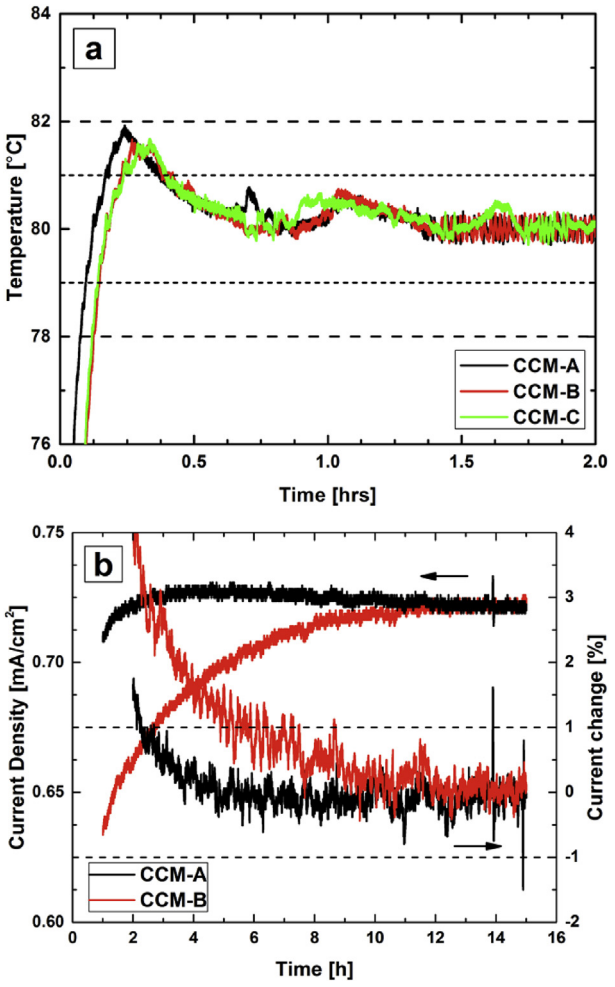

Fig. 3 – a) Temperature stabilization during warm up to 80 °C of three cells measured by one of the laboratories. b) Conditioning of CCM at 1.7 V to less than 1% variation during operation at 60 °C.

temperatures first slightly overshot the target value and then slowly approached it, achieving good stability within ±0.25 K. Note that the progression of the temperature data is highly dependent on the test station and hardware. It depends on the heat capacity of the cell, the power ratings of the heaters, pump rate of the DI water, PID control settings, and the heating strategy that was applied. It is important to highlight that care is required to understand the heating behavior of each new cell/station/heater combination as overshoots may harm the cell and temperature gradients within the cell may impact the performance observed.

Fig. 3(b) shows the performance of two CCMs measured at one of the laboratories and how it changes over the last hour during the cell conditioning step at 1.7 V and 60 °C. These were the most deviant CCMs out of the five that were tested at this laboratory. The time required for conditioning the cell to reach the desired rate of change of less than 1% was 2.25 and 5.25 h for CCM-A and CCM-B, respectively. At these times the CCMs were defined to be conditioned according to manufacturer specifications. Beyond 2.25 h the performance of CCM-A dropped slightly, while the performance of CCM-B, which was at this moment about 50 mA cm^{-2} lower was still improving. After about 12 h of operation (i.e. at the end of the conditioning period), the performance of both CCMs became identical with 0.73 A cm^{-2} at 1.7 V.

It is important to note that the rolling change of the current over the previous hour of operation was not—and typically is not—an automatically computed and online-displayed value. This implies that the decision regarding whether the CCM conditioning period was complete was left to the judgment of the operator, which may inherently carry a risk for misinterpretation. For future work, a fixed time frame and target performance may be considered to be used in addition to the rate of change. Thus challenges related to the potentially different judgment of operators at various locations would be avoided.

The performance results and standard deviation vs. current density, respectively, for a sample set of five CCMs measured at the same laboratory (Lab1) are presented in Fig. 4. This data set had the smallest deviation observed of all the five laboratories for both 60 °C and 80 °C operation. The deviation may be defined as the reproducibility of the CCMs (including experimental variabilities). Fig. 4(a) shows the VI curves for all five CCMs at a cell temperature of 60 °C. At a current density of 1 A cm^{-2} the maximum to minimum variation of the cell current was 8.6 mV. The standard deviation at this point was 0.19% and the individual cell voltages as well as the average and the standard deviation of this operating point are shown in the inset of the figure. Fig. 4(b) shows the standard deviation vs. current density. The inset of the figure shows the performance averages of the same five CCMs at 60 °C and 80 °C including their standard deviation at each operating point. The results indicate high reproducibility within the CCM batch that was used for the round robin testing.

The standard deviation remained below 0.35% in all cases. Independent from the cell temperature, it increased at a constant rate from a current density of about 0.2 A cm^{-2} to the maximum recorded current density of 2.6 A cm^{-2}. Below 0.2 A cm^{-2} the standard deviations also increased, specifically at 60 °C. This may be expected, as the power supply for a 25 cm^2 cell is required to deliver much more than the

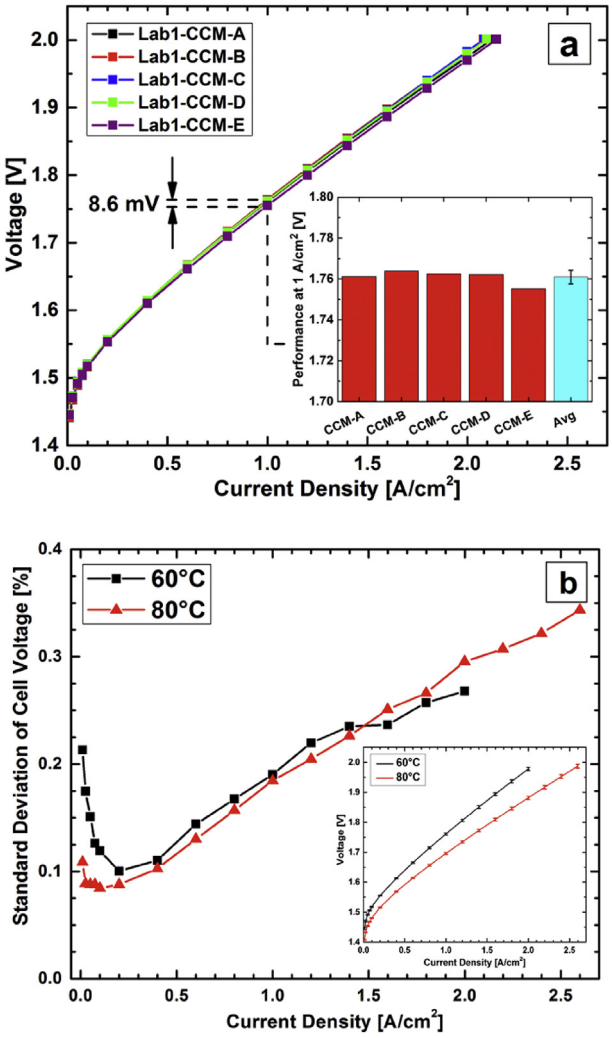

Fig. 4 – Reproducibility of five CCMs measured at the same laboratory (Lab1): a) 60 °C performance had a maximum difference of 8.6 mV at 1 A cm^{-2}. b) Averaged performances and standard deviations of the cell temperature at 60 and 80 °C.

minimum current of the test. In this particular case a power supply with a maximum current capability of 120 A was employed. At the lowest current density of 10 mA cm^{-2} (i.e. a total cell current of 250 mA), the power supply was controlled to deliver 0.2% of its maximum current capacity. It can be expected that the accuracy at the low end of the current range is less reproducible. In any case, the reproducibility of the results within the CCM batch was generally high. The reproducibility of the data measured at this laboratory (Lab 1) will serve as a reference for evaluating the reproducibility of the round robin results.

Fig. 5(a) and (b) show the averaged performance curves measured at 60 and 80 °C, respectively, at the five participating laboratories. Note that, as explained below, outlying performance curves as discussed in Fig. 6 were omitted from the calculation. The inserted bar charts show the averaged 1 A cm^{-2} performances of each lab including the overall average and standard deviation. The averaged 1 A cm^{-2}

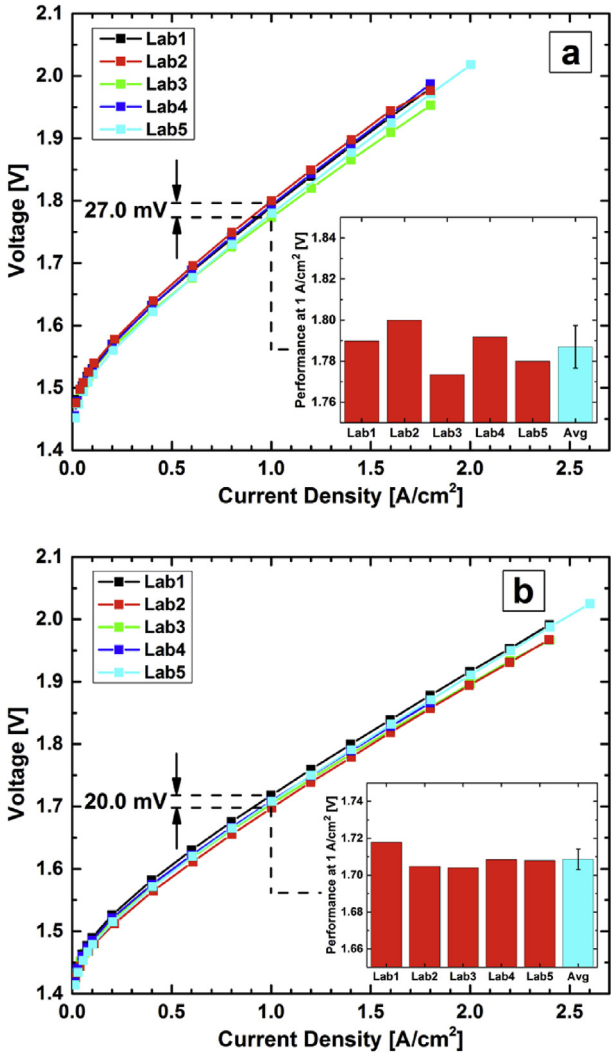

Fig. 5 – Performance comparison of experiment sets at a) 60 and b) 80 °C measured at the five laboratories.

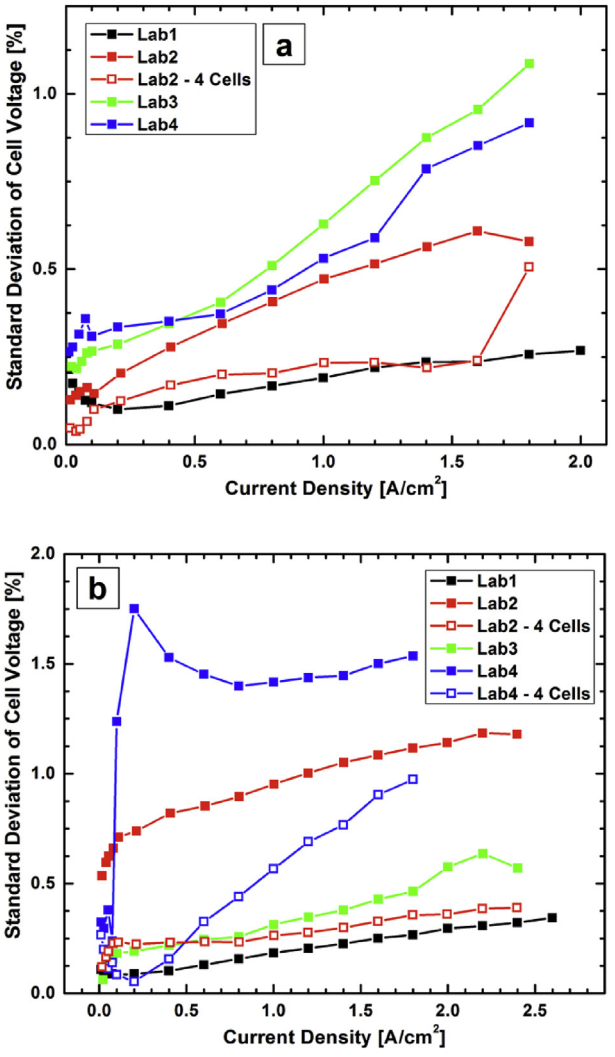

Fig. 6 – Standard deviation vs. current density for the CCM sets measured at the various laboratories. a) 60 °C and b) 80 °C.

performance across all laboratories at 60 and 80 °C was 1.787 and 1.709 V with total standard deviations of 0.010 and 0.006 V, respectively. The current density of 1 A cm^{-2} was chosen as a performance metric because it is high enough to be relevant to production and because it can be reached reasonably well with developmental cells that contain new material sets or ultra-low loadings. The figures further indicate the maximum performance deviation between the lowest and the highest average at 1 A cm^{-2}. The data show a general agreement of the results, though the observed maximum to minimum deviations exceeded those discussed in Fig. 4 by a factor of three; that is, 8.6 vs. 27 mV and 7.3 vs. 20 mV for 60 °C and 80 °C, respectively. In the insets the average performance of each laboratory, including the overall average and the standard deviation, is shown at 1 A cm^{-2}. The standard deviations were 0.58% and 0.32% for 60 °C and 80 °C, respectively. Compared to the 0.19% and 0.18% deviations observed only at Lab1, these deviations are a factor of 3.1 and 1.8 higher. This relative increase of the measurement variability is related to the operation at the various institutions using different personnel, test stations, and control strategies. It is important to note that the reproducibility improved significantly when the temperature was increased to 80 °C. This suggests that attention to the variations at lower temperatures is important to optimize the existing capability to compare data between laboratories.

Fig. 6(a) and (b) show standard deviation data from four laboratories at 60 °C and 80 °C, respectively. No standard deviation was available for the fifth laboratory, because that lab contributed a single performance curve for each temperature. Data are shown for the four labs for all five measured CCMs (solid symbols), as well as for two of the labs after removing results from one CCM (open symbols—one for 60 °C and two for 80 °C). The removed performance curves were obvious outliers. For example, the data set for 60 °C shows that the standard deviation measured over five CCMs at Lab2 reached about 0.6% at 1.6 A cm^{-2}. When removing the results of the CCM that was obviously deviating from the other four CCMs, the standard deviation dropped significantly to about 0.25% to match that of Lab1, the laboratory with the lowest observed deviations. An interesting observation is that the deviation observed at Lab3 is significantly higher at 60 °C than at 80 °C.

This may suggest that the test station of this laboratory is more optimized for operation at 80 °C and that establishing reproducible conditions at 60 °C may be more challenging. In any case, the results imply that careful control of operating conditions is key in establishing reproducible results.

For all CCMs the standard deviation in Fig. 6(a) and (b) increased with current density. If we assume that the data with the lowest deviation (i.e., the data measured at Lab1) represents the deviation inherent in the measured CCMs, then all additional deviations are introduced by the cell assembly and the operating conditions. This result suggests that experimental care needs to be taken to achieve representative results. It also suggests that multiple CCMs need to be tested before a reliable statement can be made about the performance of a particular CCM construction, catalyst material, or other component.

Fig. 7 presents the impact of changes in supplied power on the temperature stability of the cell measured by one of the laboratories. Fig. 7(a) shows a performance curve conducted from high currents to low currents during the round robin testing. Fig. 7(b) shows the resulting change of the cell, inlet and outlet temperature. As expected, the inlet temperature is independent from the power supplied to the cell as it is a controlled variable. It slowly oscillates by ±0.5 K around the target temperature of 80 °C with an approximate frequency of 2 mHz. The oscillation is not desired but specific to the hardware setup of the test station including but not limited to the PID controller settings, the power of the heaters, the insulation and the flow rate of the water. No criteria were given prior to the round robin test that regulated the allowable fluctuation of temperatures during the experiments. While in the example above the control was well below ±1 K, it may be advisable to further improve the inlet temperature variation.

Cell temperature and outlet water temperature decrease with reduction in current density until a current density of 400 mA cm^{-2} is reached. In general, it should be noted that these measurements were made using thermocouples, which, if not carefully calibrated together with the temperature controller, can result in temperature inaccuracies. The endplate temperature dropped from a maximum temperature of 81.2 °C–79.2 °C while the outlet temperature, following a similar trend, changed from 80.6 °C to 78.2 °C. At lower current densities, the endplate temperature remained stable while the outlet temperature increased again up to 79.3 °C, likely due to the PID controller adjusting the heating interval. The inlet/outlet temperature difference varied up to 2 K as shown in Fig. 7(b). This temperature variation may be very close to the borderline for precise comparison of the results as indicated by Fig. 7(c). The figure shows the performance change of a 25 cm^2 cell operated at five different temperatures ranging from 56 °C to 64 °C and measured at 2 K intervals. The performance improved by about 23 mV over the 8 K temperature span, indicating an approximately 3 mV/K performance change. In comparison, the average performance change from 60 °C to 80 °C of the results shown in Fig. 5 was 78 mV, or approximately 4 mV/K. The temperature control of the water stream fed to the cell inlet, the heat retention of the cell (i.e. the temperature of the exhaust streams) and the temperature control of the cell itself may all have an impact on the results. Calibration of all temperature control units, including their

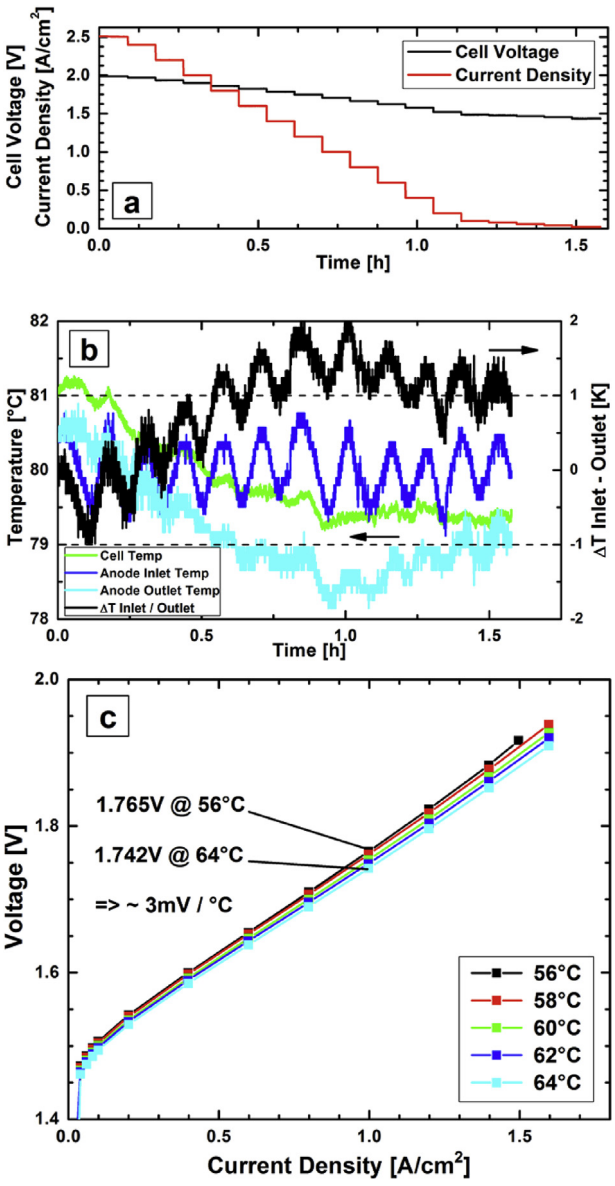

Fig. 7 – a) Applied current density steps and resulting applied voltage for high to low current performance curve. b) Temperature variation of inlet, outlet and cell temperatures during high to low current performance curve. c) Performance variation due to a 2 K inlet temperature offset at nominal 60 °C and 80 °C.

associated temperature sensors and tracking of inlet, cell and outlet temperatures seems to be one main key for establishing meaningful comparison of results. The heat retention of the cell, which is likely directly related to the applied feed stream may also impact the heat fluctuation of the cell and the variation from inlet to outlet water temperature at various current densities. Since these parameters have been left to the control of the individual laboratories, they may have contributed to the laboratory to laboratory variations.

Impedance measurement requirements during this initial round robin effort were limited to a single 1 kHz measurement at 50 mA cm^{-2}. Equipment options and measurement strategies for measuring the HFR of the cell vary widely and the

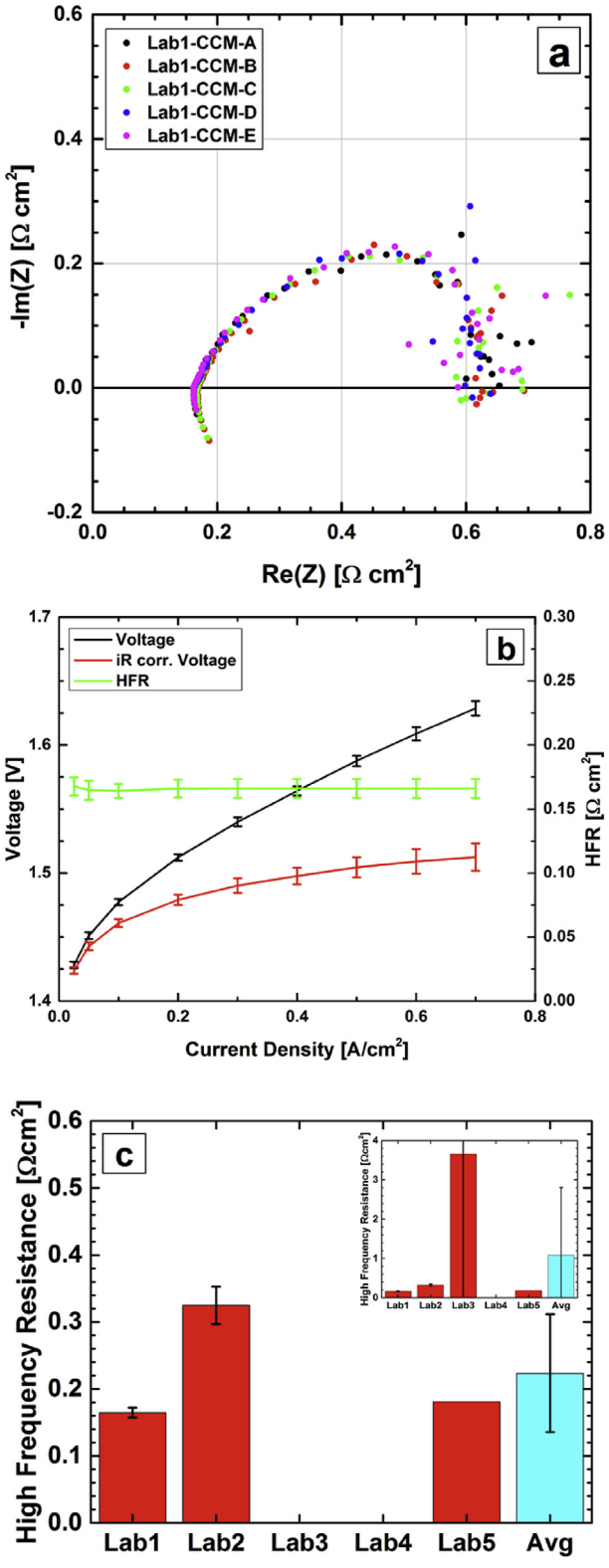

Fig. 8 – a) EIS reproducibility of five experimental sets within one laboratory. b) IR-corrected performance curve with error bars. c) Variability of 1 kHz data across the laboratories.

inclusion of the HFR measurements in the round robin test effort was meant to serve as an assessment of typical capabilities and results. Fig. 8(a) presents the electrochemical impedance spectra of five CCMs conducted at 50 mA cm^{-2} and 80 °C. Fig. 8(b) shows averaged performance, HFR and iR corrected performance curves up to 0.7 A cm^{-2} and their respective standard deviations at 80 °C. These data were successfully measured at Lab1 using a galvanostat/potentiostat/frequency response analyzer system coupled with a 20 A current booster. Note that the maximum current of the booster limited the measurements to 0.7 A cm^{-2}. The data demonstrate that reproducible EIS results can be collected; a comprehensive data set from all the laboratories however, was not available.

The individual and averaged data from laboratories Lab1, Lab2 and Lab5 are shown in Fig. 8(c) and those data additionally including Lab3 are shown in the inset of the same figure. The deviation of the HFR between the laboratories was quite significant. Only two laboratories, Lab1 and Lab5, measured values in the expected range of below 200 mΩ cm^{-2}. Results measured at Lab2 were on average about a factor of 2 times higher, and Lab3 results were on average 20 times the expected result. It is apparent by the reproducibility of the performance curves discussed in Fig. 5(a) and b) that the measured elevated HFRs may not represent actual variations of the cell resistances as they may also result from an erroneous assembly procedure. Investigations into the cell wiring setup of Lab3 revealed that the banana receptacles that are screwed into the flow-field plates of the hardware may have created additional high resistances and irreproducible contacts. Measurement cables should be contacted to the current collector plates instead. More work is necessary to identify the proper equipment, operation and calibration procedures, and training to perform accurate, reliable, and meaningful HFR and EIS data measurements.

Conclusion

The data obtained in this work corroborates the urgent need in the PEM electrolysis R&D community to establish methods and procedures that enable the meaningful comparison of in-situ results across laboratories. We, as contributors to the IEA Electrolysis Annex 30 have performed a PEM water electrolysis round robin test effort to characterize and demonstrate the comparison abilities between laboratories to date when following a minimal experimental method and equipment framework. We have aimed to identify the main critical parameters that are responsible for the reported deviations of the cell performance. The learnings are expected to feed into the development of a comprehensive test method and reference material system to be established in the near future.

A relatively tolerant set of operating conditions and test procedures was used to ensure an inclusive approach rather than the need for specific and specialized equipment. The results of measuring identical materials in an identical

hardware at five laboratories in Europe and the US identified the completeness of cell conditioning and the accuracy of temperature control as the most critical parameters that may cause performance deviation. At 60 °C and 80 °C maximum performance deviations of 27 and 20 mV, respectively, were observed between laboratories at 1 A cm^{-2}. The deviation of the results from laboratory to laboratory is about a factor of 3 times higher than the lowest deviation observed at one single lab and test station. This allowed to attribute about one-third of the deviations to inherent performance variations of the MEAs, the remaining two-thirds could be attributed to cell assembly and operating conditions.

The cell temperature reduces the performance of the cell by 3–4 mV for each °C it decreases. Slight temperature offsets and differential temperature from inlet to outlet may thus account for up to a third of the observed changes. The conditioning criteria of 1% current change per hour was found to be insufficient to ensure stationary conditions. This criterion possibly had the largest effect on the observed deviations. This parameter needs to be better defined by either choosing a significantly smaller value of, for example, 0.2% or lower, or by defining new criteria that warrant a well-defined conditioning period for the specific CCM make and model under test.

In general, the observed deviation at 80 °C was about 10 times smaller than those found in the literature, which indicates that many parameters were successfully controlled, and a large step was made towards successful performance comparison. The performance deviation generally increased with increasing current density. Interestingly, the deviation at the lower cell temperature was higher, suggesting that reproducible conditions were more difficult to achieve at 60 °C, which may likely be related to the water flow through the cell and the associated heat retention during the measurement.

Related future work of the IEA Annex 30 group will focus on defining more stringent test conditions to further improve the reproducibility and thus the capability for comparison between laboratories. The group further intends to introduce an open source test cell and titanium-based PTLs that can serve as a PEMWE reference system to the community. The cell is envisioned to be available to the public via openly shared blueprints and additionally commercially available through machining services. Both the refined conditions/protocols, commercially available reference materials and the open source cell combined will provide a reference framework that ultimately enables accurate comparison of results across the community.

Acknowledgements

The contributing laboratories would like to acknowledge funding from the following institutions: DLR and FZ-Jülich acknowledges internal funding through the Helmholtz Association. FZ Jülich also thanks Stefanie Fischer, Florian Berg, and Daniel Holtz for their support in CCM fabrication, cell assembly, and electrochemical tests. Fraunhofer ISE acknowledges Nicolas Höfling for performing the measurements, Thomas Lickert for fruitful discussion of the results, and the Federal Ministry of Education and Research of Germany for the financial support of the project "PowerMEE - Lebensdauer-und Leistungserhöhung von Polymerelektrolytmembranelektrolyseuren durch Hochleistungsmembranelektrodeneinheiten" (contract number 03SF0536D). NREL authors acknowledges funding for this work provided by the Fuel Cell Technologies Office, of the U. S. Department of Energy, Energy Efficiency and Renewable Energy under contract number DE-AC36-08-GO28308 (NREL), Technology Manager Eric Miller. The U.S. Government retains and the publisher, by accepting the article for publication, acknowledges that the U.S. Government retains a nonexclusive, paid-up, irrevocable, worldwide license to publish or reproduce the published form of this work, or allow others to do so, for U.S. Government purposes. The views and opinions of the authors expressed herein do not necessarily state or reflect those of the United States Government or any agency thereof. Neither the United States Government nor any agency thereof, nor any of their employees, makes any warranty, expressed or implied, or assumes any legal liability or responsibility for the accuracy, completeness, or usefulness of any information, apparatus, product, or process disclosed, or represents that its use would not infringe privately owned rights. Proton Onsite acknowledges internal funding for the cell testing, and additional funding provided by the Fuel Cell Technologies Office, of the U. S. Department of Energy, Energy Efficiency and Renewable Energy under contract number DE-EE0008092, Technology Manager Katie Randolph. We would further acknowledge fruitful discussions with IEA participants during and off-site of electrolysis annex 30 workshops.

REFERENCES

[1] Carmo M, et al. A comprehensive review on PEM water electrolysis. Int J Hydrog Energy 2013;38(12):4901–34.
[2] Nuttall LJ, Fickett AP, Titterington WA. Hydrogen generation by solid polymer electrolyte water electrolysis. In: Veziroğlu TN, editor. Hydrogen energy: Part A. Boston, MA: Springer US; 1975. p. 441–55.
[3] DOE-USA. DOE Multi-Year Research, Development and Demonstration Plan (2011-2020). 1]; 1-16]. Available from: https://www.energy.gov/sites/prod/files/2014/12/f19/fcto_myrdd_full_document.pdf.
[4] Buttler A, Spliethoff H. Current status of water electrolysis for energy storage, grid balancing and sector coupling via power-to-gas and power-to-liquids: a review. Renew Sustain Energy Rev 2018;82:2440–54.
[5] Rakousky C, et al. The stability challenge on the pathway to high-current-density polymer electrolyte membrane water electrolyzers. Electrochim Acta 2018;278:324–31.
[6] Paciok P, et al. On the mobility of carbon-supported platinum nanoparticles towards unveiling cathode degradation in water electrolysis. J Power Sources 2017;365:53–60.
[7] Rakousky C, et al. Polymer electrolyte membrane water electrolysis: restraining degradation in the presence of fluctuating power. J Power Sources 2017;342:38–47.
[8] Rakousky C, et al. An analysis of degradation phenomena in polymer electrolyte membrane water electrolysis. J Power Sources 2016;326:120–8.
[9] Mergel J, Fritz DL, Carmo M. Stack technology for PEM electrolysis. In: Emonts DSaDB, editor. Hydrogen science and engineering : materials, processes, systems and technology; 2016.

[10] Wang L, et al. Improving the activity and stability of Ir catalysts for PEM electrolyzer anodes by SnO2:Sb aerogel supports: does V addition play an active role in electrocatalysis? J Mater Chem 2017;5(7):3172–8.
[11] Lettenmeier P, et al. Low-cost and durable bipolar plates for proton exchange membrane electrolyzers. Sci Rep 2017;7:44035.
[12] Toops TJ, et al. Evaluation of nitrided titanium separator plates for proton exchange membrane electrolyzer cells. J Power Sources 2014;272:954–60.
[13] Gago AS, et al. Protective coatings on stainless steel bipolar plates for proton exchange membrane (PEM) electrolysers. J Power Sources 2016;307:815–25.
[14] Mo J, et al. Thin liquid/gas diffusion layers for high-efficiency hydrogen production from water splitting. Appl Energy 2016;177:817–22.
[15] Lettenmeier P, et al. Comprehensive investigation of novel pore-graded gas diffusion layers for high-performance and cost-effective proton exchange membrane electrolyzers. Energy Environ Sci 2017;10(12):2521–33.
[16] Schalenbach M, et al. Acidic or alkaline? Towards a new perspective on the efficiency of water electrolysis. J Electrochem Soc 2016;163(11):F3197–208.
[17] US fuel cell Council (USFCC) document number 04-011.
[18] US fuel cell Council (USFCC) document number 05-014B.2.
[19] https://www.energy.gov/eere/fuelcells/downloads/fuel-cell-technologies-office-multi-year-research-development-and-22.
[20] Zhao S, et al. Highly active, durable dispersed iridium nanocatalysts for PEM water electrolyzers. J Electrochem Soc 2018;165(2):F82–9.
[21] Yang GQ, et al. Fully printed and integrated electrolyzer cells with additive manufacturing for high-efficiency water splitting. Appl Energy 2018;215:202–10.
[22] Toghyani S, et al. Thermal and electrochemical analysis of different flow field patterns in a PEM electrolyzer. Electrochim Acta 2018;267:234–45.
[23] Tijani AS, Kamarudin NAB, Mazlan FAB. Investigation of the effect of charge transfer coefficient (CTC) on the operating voltage of polymer electrolyte membrane (PEM) electrolyzer. Int J Hydrog Energy 2018;43(19):9119–32.
[24] Park H, et al. Direct fabrication of gas diffusion cathode by pulse electrodeposition for proton exchange membrane water electrolysis. Appl Surf Sci 2018;444:303–11.
[25] Li YF, et al. In-situ investigation of bubble dynamics and two-phase flow in proton exchange membrane electrolyzer cells. Int J Hydrog Energy 2018;43(24):11223–33.
[26] Lee C, et al. The effect of cathode nitrogen purging on cell performance and in operando neutron imaging of a polymer electrolyte membrane electrolyzer. Electrochim Acta 2018;279:91–8.
[27] Kumar SS, et al. Preparation of RuxPd1-xO2 electrocatalysts for the oxygen evolution reaction (OER) in PEM water electrolysis. Ionics 2018;24(8):2411–9.
[28] Kim JH, et al. Electrodeposited molybdenum sulfide as a cathode for proton exchange membrane water electrolyzer. J Power Sources 2018;392:69–78.
[29] Kim H, et al. A transition metal oxysulfide cathode for the proton exchange membrane water electrolyzer. Appl Catal B Environ 2018;232:93–100.
[30] Kasian O, et al. The common intermediates of oxygen evolution and dissolution reactions during water electrolysis on iridium. Angew Chem Int Ed 2018;57(9):2488–91.
[31] Kang ZY, et al. Novel thin/tunable gas diffusion electrodes with ultra-low catalyst loading for hydrogen evolution reactions in proton exchange membrane electrolyzer cells. Nanomater Energy 2018;47:434–41.
[32] Jorge AB, et al. Carbon nitride materials as efficient catalyst supports for proton exchange membrane water electrolyzers. Nanomaterials 2018;8(6).
[33] Immerz C, et al. Effect of the MEA design on the performance of PEMWE single cells with different sizes. J Appl Electrochem 2018;48(6):701–11.
[34] Choe S, et al. Electrodeposited IrO2/Ti electrodes as durable and cost-effective anodes in high-temperature polymer-membrane-electrolyte water electrolyzers. Appl Catal B Environ 2018;226:289–94.
[35] Bromberger K, et al. Hydraulic ex situ through-plane characterization of porous transport layers in PEM water electrolysis cells. Int J Hydrog Energy 2018;43(5):2556–69.
[36] Bernt M, Siebel A, Gasteiger HA. Analysis of voltage losses in PEM water electrolyzers with low platinum group metal loadings. J Electrochem Soc 2018;165(5):F305–14.
[37] Zeng YC, et al. A cost-effective nanoporous ultrathin film electrode based on nanoporous gold/IrO2 composite for proton exchange membrane water electrolysis. J Power Sources 2017;342:947–55.
[38] Yang GQ, et al. Additive manufactured bipolar plate for high-efficiency hydrogen production in proton exchange membrane electrolyzer cells. Int J Hydrog Energy 2017;42(21):14734–40.
[39] Wang L, et al. Highly active anode electrocatalysts derived from electrochemical leaching of Ru from metallic Ir0.7Ru0.3 for proton exchange membrane electrolyzers. Nanomater Energy 2017;34:385–91.
[40] Verdin B, et al. Operando current mapping on PEM water electrolysis cells. Influence of mechanical stress. Int J Hydrog Energy 2017;42(41):25848–59.
[41] Trinke P, Bensmann B, Hanke-Rauschenbach R. Experimental evidence of increasing oxygen crossover with increasing current density during PEM water electrolysis. Electrochem Commun 2017;82:98–102.
[42] Suermann M, et al. Influence of operating conditions and material properties on the mass transport losses of polymer electrolyte water electrolysis. J Electrochem Soc 2017;164(9):F973–80.
[43] Siracusano S, et al. Enhanced performance and durability of low catalyst loading PEM water electrolyser based on a short-side chain perfluorosulfonic ionomer. Appl Energy 2017;192:477–89.
[44] Siracusano S, et al. Sulfated titania as additive in Nafion membranes for water electrolysis applications. Int J Hydrog Energy 2017;42(46):27851–8.
[45] Siracusano S, et al. The influence of iridium chemical oxidation state on the performance and durability of oxygen evolution catalysts in PEM electrolysis. J Power Sources 2017;366:105–14.
[46] Shi Y, et al. Fabrication of membrane electrode assemblies by direct spray catalyst on water swollen Nafion membrane for PEM water electrolysis. Int J Hydrog Energy 2017;42(42):26183–91.
[47] Lv H, et al. Activity of IrO2 supported on tantalum-doped TiO2 electrocatalyst for solid polymer electrolyte water electrolyzer. RSC Adv 2017;7(64):40427–36.
[48] Kim H, et al. Non-precious metal electrocatalysts for hydrogen production in proton exchange membrane water electrolyzer. Appl Catal B Environ 2017;206:608–16.
[49] Kim H, et al. An extremely low Pt loading cathode for a highly efficient proton exchange membrane water electrolyzer. Nanoscale 2017;9(48):19045–9.
[50] Karimi F, Peppley BA. Metal carbide and oxide supports for iridium-based oxygen evolution reaction electrocatalysts for polymer-electrolyte-membrane water electrolysis. Electrochim Acta 2017;246:654–70.

[51] Kang ZY, et al. Thin film surface modifications of thin/tunable liquid/gas diffusion layers for high-efficiency proton exchange membrane electrolyzer cells. Appl Energy 2017;206:983–90.
[52] Hao CP, et al. Investigation of V-doped TiO2 as an anodic catalyst support for SPE water electrolysis. Int J Hydrog Energy 2017;42(15):9384–95.
[53] Grigoriev SA, Bessarabov DG, Fateev VN. Degradation mechanisms of MEA characteristics during water electrolysis in solid polymer electrolyte cells. Russ J Electrochem 2017;53(3):318–23.
[54] Fujigaya T, et al. A highly efficient and durable carbon nanotube-based anode electrocatalyst for water electrolyzers. J Mater Chem 2017;5(21):10584–90.
[55] Chourashiya MG, Urakawa A. Solution combustion synthesis of highly dispersible and dispersed iridium oxide as an anode catalyst in PEM water electrolysis. J Mater Chem 2017;5(10):4774–8.
[56] Chang JF, et al. Core-shell structured Ni12P5/Ni-3(PO4)(2) hollow spheres as difunctional and efficient electrocatalysts for overall water electrolysis. Appl Catal B Environ 2017;204:486–96.
[57] Babic U, et al. Review-identifying critical gaps for polymer electrolyte water electrolysis development. J Electrochem Soc 2017;164(4):F387–99.
[58] Lettenmeier P, et al. Towards developing a backing layer for proton exchange membrane electrolyzers. J Power Sources 2016;311:153–8.
[59] Kus P, et al. Magnetron sputtered Ir thin film on TiC-based support sublayer as low-loading anode catalyst for proton exchange membrane water electrolysis. Int J Hydrog Energy 2016;41(34):15124–32.
[60] Han B, et al. Effects of membrane electrode assembly properties on two-phase transport and performance in proton exchange membrane electrolyzer cells. Electrochim Acta 2016;188:317–26.
[61] Fouda-Onana F, et al. Investigation on the degradation of MEAs for PEM water electrolysers part I: effects of testing conditions on MEA performances and membrane properties. Int J Hydrog Energy 2016;41(38):16627–36.
[62] Di Giovanni C, et al. Low-cost nanostructured iron sulfide electrocatalysts for PEM water electrolysis. ACS Catal 2016;6(4):2626–31.
[63] Bernt M, Gasteiger HA. Influence of ionomer content in IrO2/TiO2 electrodes on PEM water electrolyzer performance. J Electrochem Soc 2016;163(11):F3179–89.
[64] Zhao S, et al. Calculating the electrochemically active surface area of iridium oxide in operating proton exchange membrane electrolyzers. J Electrochem Soc 2015;162(12):F1292–8.
[65] Siracusano S, et al. Nanosized IrOx and IrRuOx electrocatalysts for the O-2 evolution reaction in PEM water electrolysers. Appl Catal B Environ 2015;164:488–95.
[66] Siracusano S, et al. Performance of a PEM water electrolyser combining an IrRu-oxide anode electrocatalyst and a short-side chain Aquivion membrane. Int J Hydrog Energy 2015;40(42):14430–5.
[67] Selamet OF, Ergoktas MS. Effects of bolt torque and contact resistance on the performance of the polymer electrolyte membrane electrolyzers. J Power Sources 2015;281:103–13.
[68] Oh HS, et al. Oxide-supported Ir nanodendrites with high activity and durability for the oxygen evolution reaction in acid PEM water electrolyzers. Chem Sci 2015;6(6):3321–8.
[69] Ng JWD, et al. Polymer electrolyte membrane electrolyzers utilizing non-precious Mo-based hydrogen evolution catalysts. Chemsuschem 2015;8(20):3512–9.
[70] Liu GY, et al. An oxygen evolution catalyst on an antimony doped tin oxide nanowire structured support for proton exchange membrane liquid water electrolysis. J Mater Chem 2015;3(41):20791–800.
[71] Lee BS, et al. Development of electrodeposited IrO2 electrodes as anodes in polymer electrolyte membrane water electrolysis. Appl Catal B Environ 2015;179:285–91.
[72] Brightman E, et al. In situ characterisation of PEM water electrolysers using a novel reference electrode. Electrochem Commun 2015;52:1–4.
[73] Albert A, et al. Radiation-grafted polymer electrolyte membranes for water electrolysis cells: evaluation of key membrane properties. ACS Appl Mater Interfaces 2015;7(40):22203–12.
[74] van der Merwe J, et al. Characterisation tools development for PEM electrolysers. Int J Hydrog Energy 2014;39(26):14212–21.
[75] Sun SC, et al. Investigations on degradation of the long-term proton exchange membrane water electrolysis stack. J Power Sources 2014;267:515–20.
[76] Skulimowska A, et al. Proton exchange membrane water electrolysis with short-side-chain Aquivion (R) membrane and IrO2 anode catalyst. Int J Hydrog Energy 2014;39(12):6307–16.
[77] Siracusano S, et al. Performance analysis of short-side-chain Aquivion (R) perfluorosulfonic acid polymer for proton exchange membrane water electrolysis. J Membr Sci 2014;466:1–7.
[78] Rozain C, Millet P. Electrochemical characterization of polymer electrolyte membrane water electrolysis cells. Electrochim Acta 2014;131:160–7.
[79] Puthiyapura VK, et al. Investigation of supported IrO2 as electrocatalyst for the oxygen evolution reaction in proton exchange membrane water electrolyser. Int J Hydrog Energy 2014;39(5):1905–13.
[80] Puthiyapura VK, et al. Physical and electrochemical evaluation of ATO supported IrO2 catalyst for proton exchange membrane water electrolyser. J Power Sources 2014;269:451–60.
[81] Liu GY, et al. A novel catalyst coated membrane embedded with Cs-substituted phosphotungstates for proton exchange membrane water electrolysis. Int J Hydrog Energy 2014;39(27):14531–9.
[82] Liu GY, et al. Nanosphere-structured composites consisting of Cs-substituted phosphotungstates and antimony doped tin oxides as catalyst supports for proton exchange membrane liquid water electrolysis. Int J Hydrog Energy 2014;39(5):1914–23.
[83] Wang XY, et al. Preparation and characterization of partial-cocrystallized catalyst-coated membrane for solid polymer electrolyte water electrolysis. Int J Hydrog Energy 2013;38(22):9057–64.
[84] Su HN, Linkov V, Bladergroen BJ. Membrane electrode assemblies with low noble metal loadings for hydrogen production from solid polymer electrolyte water electrolysis. Int J Hydrog Energy 2013;38(23):9601–8.
[85] Li GF, et al. Highly effective IrxSn1-xO2 electrocatalysts for oxygen evolution reaction in the solid polymer electrolyte water electrolyser. Phys Chem Chem Phys 2013;15(8):2858–66.
[86] Ito H, et al. Influence of pore structural properties of current collectors on the performance of proton exchange membrane electrolyzer. Electrochim Acta 2013;100:242–8.
[87] Briguglio N, et al. Design and testing of a compact PEM electrolyzer system. Int J Hydrog Energy 2013;38(26):11519–29.
[88] Arico AS, et al. Polymer electrolyte membrane water electrolysis: status of technologies and potential applications in combination with renewable power sources. J Appl Electrochem 2013;43(2):107–18.